Electronic Supplementary Information

Reconfigurable Amplified Circularly Polarized Photo/Electro-luminescence from Simple Solution Self-assembly of a Chiral Deep-blue Fluorene-based Conjugated Polymer

Hao Li, [a] Mengna Yu,*[a] Manman Luo, [a] Yang Li, [a] Zixuan Chen, [b] Jiangqiang He, [a] Menghan Wu, [a] Yiren Liu, [a] Kuande Wang, [a] Xiaozhi Zhan, [c] Yunlong Zhang, [a] Jiabin Gu, [a] Youxuan Zheng, [b] Shasha Wang, [a] Zhikuan Chen, [d] Quanyou Feng* [a] and Linghai Xie* [a, e]

[a] Centre for Molecular Systems and Organic Devices (CMSOD), State Key Laboratory of Flexible Electronics (LoFE) & Institute of Advanced Materials (IAM), Nanjing University of Posts & Telecommunications, 9 Wenyuan Road, Nanjing 210023, China

[b] State Key Laboratory of Coordination Chemistry, Jiangsu Key Laboratory of Advanced Organic Materials, School of Chemistry and Chemical Engineering, Nanjing University, Nanjing, 210023, P. R. China

[c] Spallation Neutron Source Science Center, Dongguan 523803, China; Institute of High Energy Physics, Chinese Academy of Sciences, Beijing 100049, China

[d] Key laboratory of Flexible Electronics of Zhejiang Province, Ningbo Institute of Northwestern Polytechnical University, 218 Qingyi Road, Ningbo 315103, China

[e] School of Flexible Electronics (SoFE) and Henan Institute of Flexible Electronics (HIFE), Henan University, 379 Mingli Road, Zhengzhou 450046, China

Contents

Materials

All solvents and reagents were purchased from commercial suppliers and used without further purification unless otherwise specified. Dichloromethane (DCM) was dried over anhydrous sodium at room temperature. Tetrahydrofuran and chloroform were dried over sodium benzophenone ketyl anion radical and distilled under a dry nitrogen atmosphere immediately prior to use. Anhydrous sodium sulfate, chloroform, DMF, KOH, acetone, K_2CO_3 and toluene were purchased from Sinopharm Chemical Reagent Co, Ltd. without further purification. 2,7-dibromo-9-fluorenone (2,7-DBrFO), bromobenzene, sodium percarbonate, trifluoroacetic acid, boron(tri)fluoride etherate, TBAB, phenylmagnesium bromide, iodomethane, boron tribromide, (S)-1-bromo-2-methylbutane, 2,2'-bipyridine, 1,5-cyclooctadiene, $Ni(COD)_2$ and 1-bromooctane were purchased from Aldrich Chemical Co.

General Measurement and Characterization

X-ray diffraction (XRD) measurements were performed using a Bruker D8 Quest X-ray diffractometer. Single-crystal crystallography data were collected on a Bruker 2000 CCD area detector (photon 100 surface detector) with graphite-monochromated Mo Kα radiation. MALDI-TOF-MS was conducted using an Autoflex Speed MALDI-TOF instrument. ^{1}H and ^{13}C NMR data were obtained on a Bruker 400 MHz NMR Fourier transform spectrometer at 20 ^{o}C, with operating frequencies of 400 MHz for ^{1}H and 100 MHz for ^{13}C NMR, respectively. GPC analysis was performed on an HP1100 HPLC system equipped with 7911GP-502 and GPC columns using polystyrene standards for

calibration. Tetrahydrofuran (THF) was selected as the eluent (solution concentration 0.8 mg mL^{-1}) at a flow rate of 1.0 mL min^{-1}. Thermogravimetric analysis (TGA) was carried out using a STA 2500 Regulus instrument (NETZSCH Instruments). Differential scanning calorimetry (DSC) data were measured on a DSC214 Polyma instrument (NETZSCH Instruments) with a temperature range of 25 to 350 °C and a heating rate of 10 °C min^{-1}. UV-visible absorption and transmittance spectra were recorded on a PerkinElmer Lamda35 spectrophotometer at room temperature. Photoluminescence spectra were measured using a Shimadzu RF-6000 spectrofluorometer. Fluorescence lifetime and quantum yield measurements were performed on an Edinburgh FLS920 steady-state and transient fluorescence spectrometer. Circular dichroism (CD) spectra were acquired on a Jasco J-810 circular dichroism spectrometer with "Standard" sensitivity. Circularly polarized luminescence (CPL) properties were measured using a JASCO CPL-300 instrument, with a fixed DC voltage of approximately 0.5 V. The surface morphology of all self-assembly films was characterized by SEM (Hitachi, S-4800) at an accelerating voltage of 5 kV. Powder-XRD patterns were obtained using a D8 Advance A25 diffractometer. X-ray reflectivity (XRR) measurements were performed on a SmartLab Series X-ray diffractometer. Neutron reflectometry (NR) measurements were performed on the multipurpose reflectometer at the China Spallation Neutron Source (CSNS, MR beamline). Angle-dependent reflectance spectra were measured using a micro-region angle-resolved spectrum system (ARMS-U2, Ideaoptics, China). A halogen lamp served as the visible light source, and measurements were performed in constant angle incidence and reflection (CAR) mode, where the incidence angle

equaled the reflection angle. An aluminum mirror was used as the standard, and a black sponge was used for background correction to convert count mode spectra to reflectance spectra. All self-assembly films were deposited on quartz substrates for these measurements. Cyclic voltammetry (CV) studies were taken using a CHI650E electrochemical workstation in a three-electrode configuration, comprising a platinum sheet working electrode, a platinum wire counter electrode, and a silver/silver nitrate (Ag/Ag^+) reference electrode. The calculation process of HOMO and LUMO energy levels: HOMO = – (E_{ox}^{onset} – 0.03 V) – 4.8 eV; LUMO = – (E_{red}^{onset} – 0.03 V) – 4.8 eV.

Fabrication and Characterization of PLEDs

All PLEDs devices were fabricated and characterized following the process outlined below. The ITO substrates (obtained from Advanced Election Technology Co.,Ltd) were cleaned sequentially in an ultrasonic bath using detergent, acetone, ethanol, dichloromethane and deionized water. They were then dried in an oven at 120 °C for 2 hours and subsequently treated with ultraviolet ozone for 10 minutes prior to spin-coating. Firstly, a 40 nm thick layer of PEDOT: PSS was spin-coated at 1500 rpm for 30 seconds, followed by annealing at 120 °C for 20 minutes. Subsequently, the emissive layer was deposited by spin-coating a toluene solution (10 mg mL^{-1}) of the target polymer at 1500 rpm for 30 seconds, with subsequent annealing at 120 °C for 20 minutes in a nitrogen-filled glovebox. The resulting polymer film thickness was approximately 40 nm. Finally, the remaining layers, consisting of 25 nm of TPBi, 1 nm

of LiF and 100 nm of Al, were deposited through thermal evaporation under a pressure below 1×10^{-5} mbar. J-L-V curves were recorded using a Keithley source meter (model 2602) coupled with a luminance meter. EL spectra were measured using a PR-655 spectrophotometer. All measurements were performed under ambient conditions at room temperature.

The synthesis procedures for DBrChDPF

In a 1000 mL round-bottom flask equipped with a magnetic stir bar, the reaction components were sequentially introduced, including MOH (2 g, 4.07 mmol, prepared according to our group's previous report [1,2]), (S)-1-bromo-2-methylbutane (1.23 g, 8.14 mmol), TBAB (1.31 g, 4.07 mmol), and K_2CO_3 (5.62 g, 40.7 mmol). The reaction system was purged with nitrogen gas through three consecutive degassing cycles. Subsequently, anhydrous acetone (400 mL) was added, and the reaction mixture was heated to 70 °C with constant stirring for 24 hours under nitrogen atmosphere. After completion of the reaction, the mixture was quenched by pouring into water, followed by triple extraction with dichloromethane. The organic extracts were dried over Na_2SO_4, and the solvent was removed under reduced pressure. The crude product was purified by flash column chromatography on silica gel, employing a mixed solvent system of petroleum ether and methylene chloride (8:1 v/v) as the eluent, yielding the desired product as a pale yellow solid (1.44 g, 63.2% yield). The molecular structure of the target compound was confirmed through ^{1}H NMR, ^{13}C NMR and MALDI-TOF-MS.

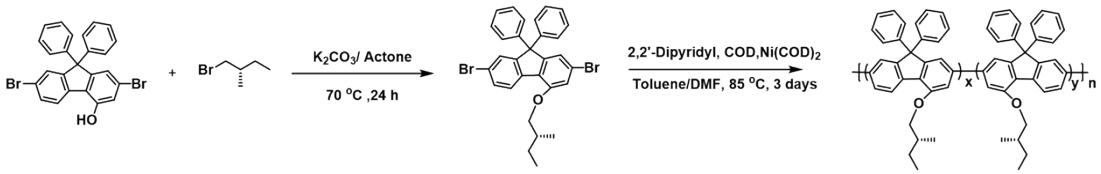

Scheme S1. Synthesis procedure for PChDPF.

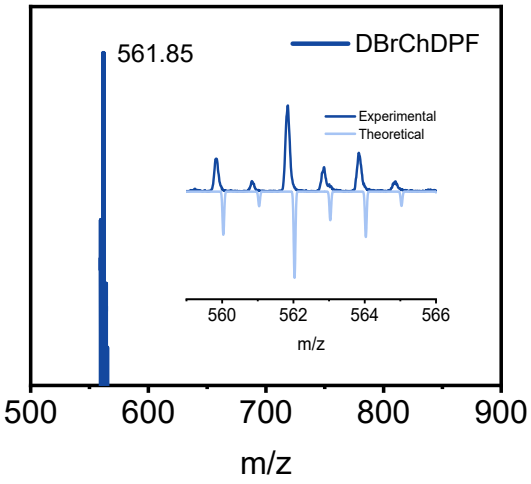

Figure S1. MALDI-TOF-MS spectra of DBrChDPF.

MALDI-TOF-MS: *m/z* calcd for $C_{30}H_{26}Br_2O$: 562.03; found: 561.85.

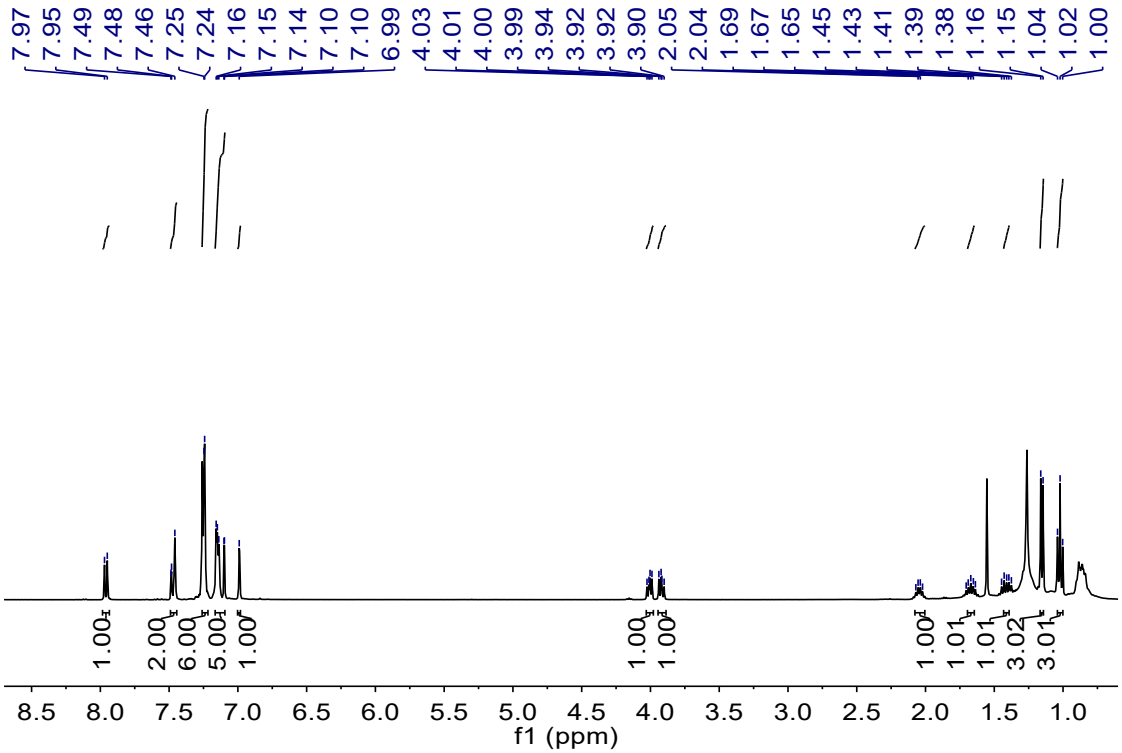

Figure S2. ^{1}H NMR spectrum of DBrChDPF in $CDCl_3$.

^{1}H NMR (400 MHz, $CDCl_3$) δ 7.97-7.95 (d, *J* = 8 Hz, 1H), 7.49-7.46 (t, *J* = 11.6 Hz, 2H), 7.25-7.24 (m, 6H), 7.16-7.10 (m, 5H), 6.99 (s, 1H), 4.03-3.99 (m, 1H), 3.94-3.90 (m, 1H), 2.07-2.02 (m, 1H), 1.70-1.64 (m, 1H), 1.45-1.38 (m, 1H), 1.16-1.15 (d, *J* = 6.8 Hz, 3H), 1.04-1.00 (t, *J* = 14.8 Hz, 3H).

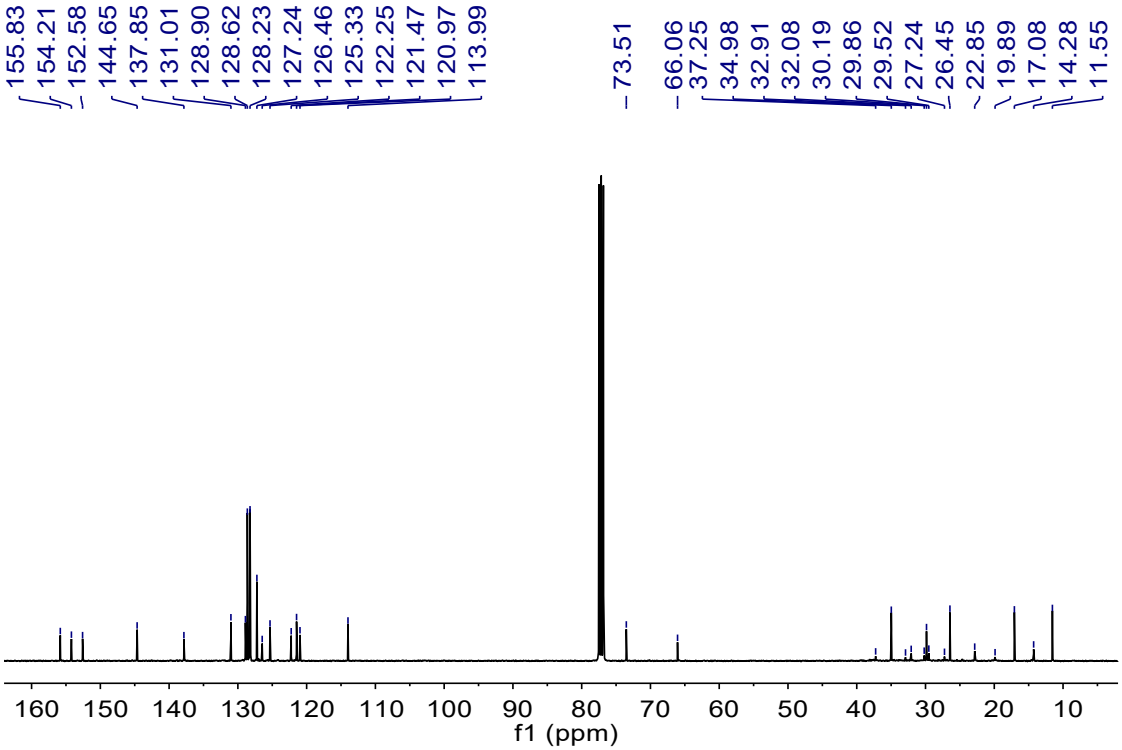

Figure S3. ^{13}C NMR spectrum of DBrChDPF in $CDCl_3$.

^{13}C NMR (100 MHz, CDCl3) δ 155.83, 154.21, 152.58, 144.65, 137.85, 131.01, 128.90, 128.62, 128.23, 127.24, 126.46, 125.33, 122.25, 121.47, 120.97, 113.99, 73.51, 66.06, 37.25, 34.98, 32.91, 32.08, 30.19, 29.86, 29.52, 27.24, 26.45, 22.85, 19.89, 17.08, 14.28, 11.55.

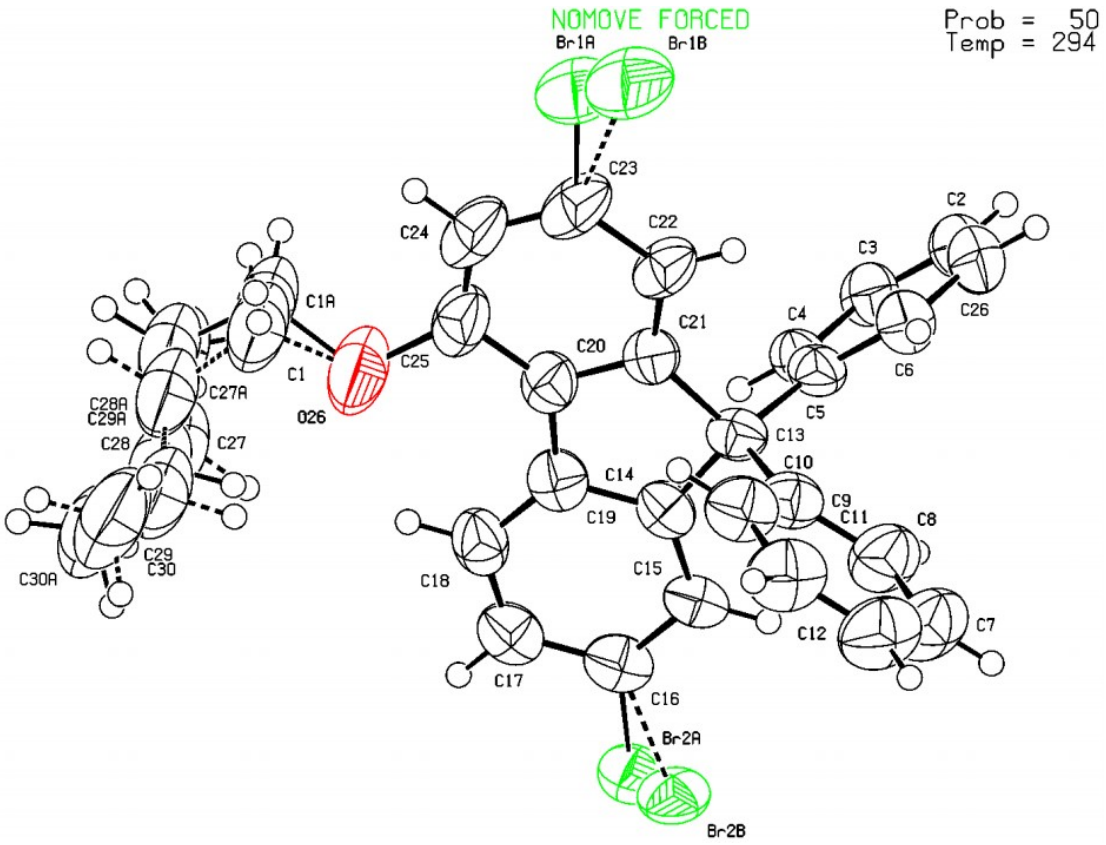

Figure S4. ORTEP of the DBrChDPF single crystal (Related to Scheme 1).

Bond precision: C-C = 0.0134 A Wavelength=0.71076

Cell: a=10.153(3) b=11.285(3) c=13.333(4)
alpha=102.153(5) beta=109.897(6) gamma=107.222(5)
Temperature: 294 K

	Calculated	Reported
Volume	1287.0(6)	1286.9(6)
Space group	P -1	P -1
Hall group	-P 1	-P 1
Moiety formula	C30 H26 Br2 O	C30 H26 Br2 O
Sum formula	C30 H26 Br2 O	C30 H26 Br2 O
Mr	562.31	562.33
Dx,g cm-3	1.451	1.451
Z	2	2
Mu (mm-1)	3.169	3.169
F000	568.0	568.0
F000'	567.07	
h,k,lmax	11,13,15	11,13,15
Nref	4386	4210
Tmin,Tmax	0.472,0.939	0.539,0.745
Tmin'	0.327	

Correction method= # Reported T Limits: Tmin=0.539 Tmax=0.745
AbsCorr = MULTI-SCAN

Data completeness= 0.960 Theta(max)= 24.711

R(reflections)= 0.1225(2161) wR2(reflections)= 0.2697(4210)

S = 0.989 Npar= 318

Table S1. The crystal information of DBrChDPF single crystal (Related to Scheme 1).

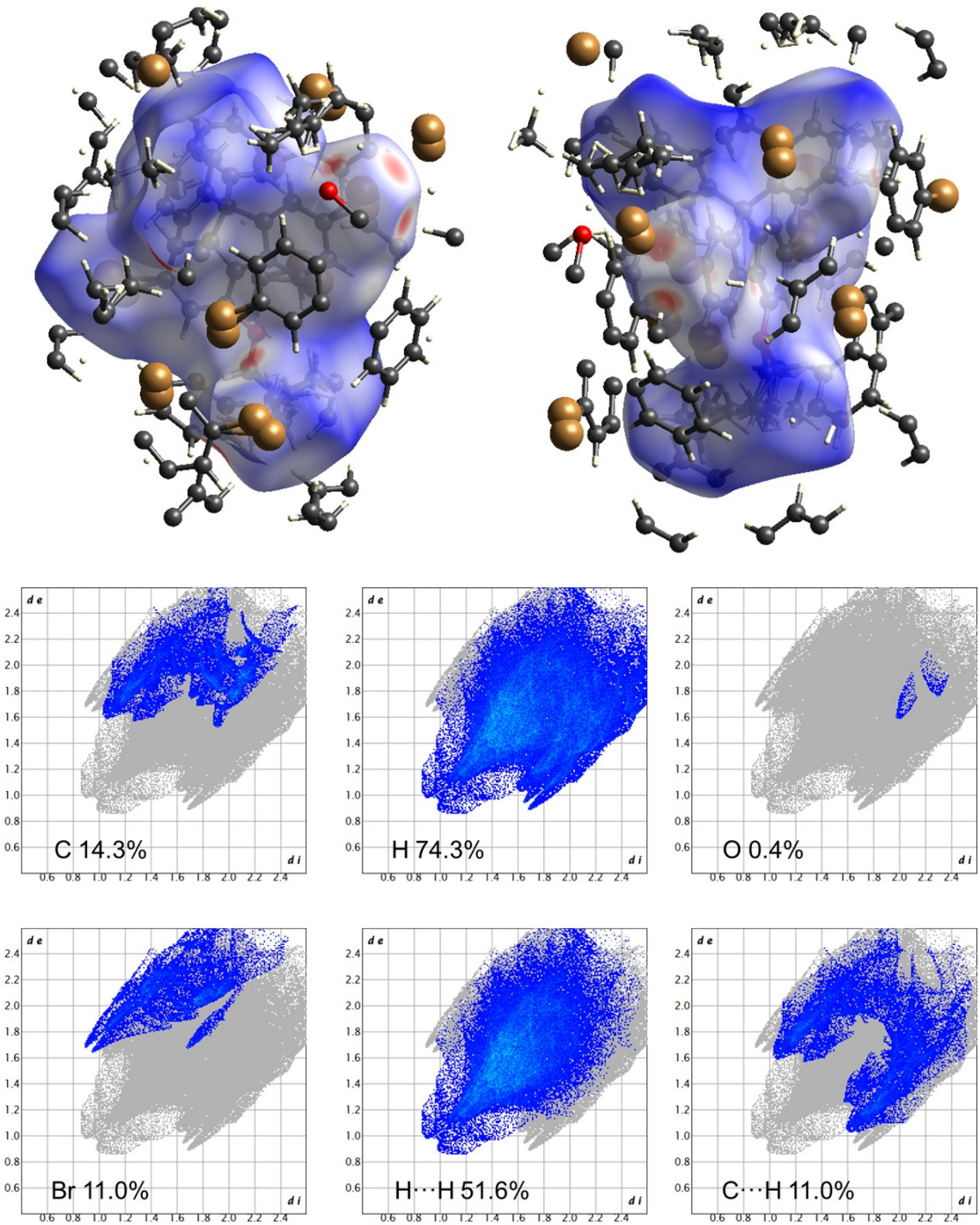

Figure S5. Hirshfeld surface analysis of the DBrChDPF single crystal by CrystalExplorer.

The synthesis procedures for target polymer PChDPF

In a nitrogen-purged 100 mL Schlenk flask equipped with a magnetic stir bar, the monomer (500 mg, 0.89 mmol) was dissolved in a mixture of ultra-dry toluene (50 mL) and ultra-dry N,N-dimethylformamide (DMF, 10 mL). To this solution, 2,2'-Dipyridyl (1.39 g) and 1,2,5,6-cyclooctanetetraylidene (1000 mg) were added sequentially. The reaction system was purged with nitrogen gas through three consecutive degassing cycles. The mixture was then heated to 90 °C under nitrogen atmosphere and stirred in the absence of light for 30 minutes. Following this, 1,5-cyclooctadiene (1.2 mL) was added, and the polymerization was allowed to proceed in the dark for 4 days with constant stirring. Upon completion of the polymerization, bromobenzene (1 mL) was added to the flask, and the mixture was refluxed for 12 hours. The reaction mixture was then cooled to ambient temperature and filtered through a sintered glass funnel to remove any insoluble residues. The filtrate was purified by flash column chromatography using Al_2O_3 as the stationary phase and THF as the mobile phase. The collected fractions containing the polymer were concentrated under reduced pressure, and the polymer was precipitated by dropwise addition into cold methanol. The resulting solid was collected by filtration and subjected to Soxhlet extraction with acetone to remove oligomers and catalyst residues. The powder was dried under vacuum, yielding the target polymer PChDPF as a fine powder with a yield of 40%-50%.

Several solution processing methods used for target polymer PChDPF

Polymer-toluene solution: A homogeneous polymer solution was prepared by dissolving 10 mg of PChDPF in 1 mL of toluene. The mixture was gently heated to facilitate complete dissolution, followed by cooling to room temperature, yielding a transparent polymer-toluene solution.

Spin coating film: 100 μL of the polymer-toluene solution (10 mg mL^{-1}) was deposited onto a quartz substrate. The film was formed by spin-coating using a KW-4A spin coater under the following conditions: 1500 rpm rotational speed with an acceleration rate of 800 rpm s^{-1}, maintained for 60 seconds.

Drop-casting film: 100 μL of the polymer-toluene solution (10 mg mL^{-1}) was dispensed onto a quartz substrate. The film was allowed to form through natural solvent evaporation at ambient conditions, typically requiring approximately 10 minutes for complete solvent removal.

Solvent-casting film: 100 μL of the polymer-toluene solution (10 mg mL^{-1}) was deposited onto a quartz substrate, which was then transferred to a petri dish. The dish was partially filled with toluene to create a solvent-rich atmosphere and loosely sealed to control evaporation rate. The slow solvent evaporation process over 5 days facilitated the formation of well-ordered solvent-casting films.

Bad solvent induced microsphere film: 10 mg of PChDPF was dissolved in 1 mL of clean 1,2-dichloroethane at 75~80 °C with constant stirring. Ethanol was then introduced dropwise as a non-solvent to induce microsphere formation. After aging at 25 °C for 5 minutes, 100 μL of the microsphere-containing solution was deposited onto the quartz substrate, allowing solvent evaporation to produce microsphere films.

Solvent-annealing film: The microsphere films were subjected to solvent annealing by placing them in a toluene-saturated environment within a partially sealed petri dish. The controlled solvent vapor exposure over 5 days enabled molecular chain rearrangement and self-assembly, resulting in the formation of solvent-annealed films.

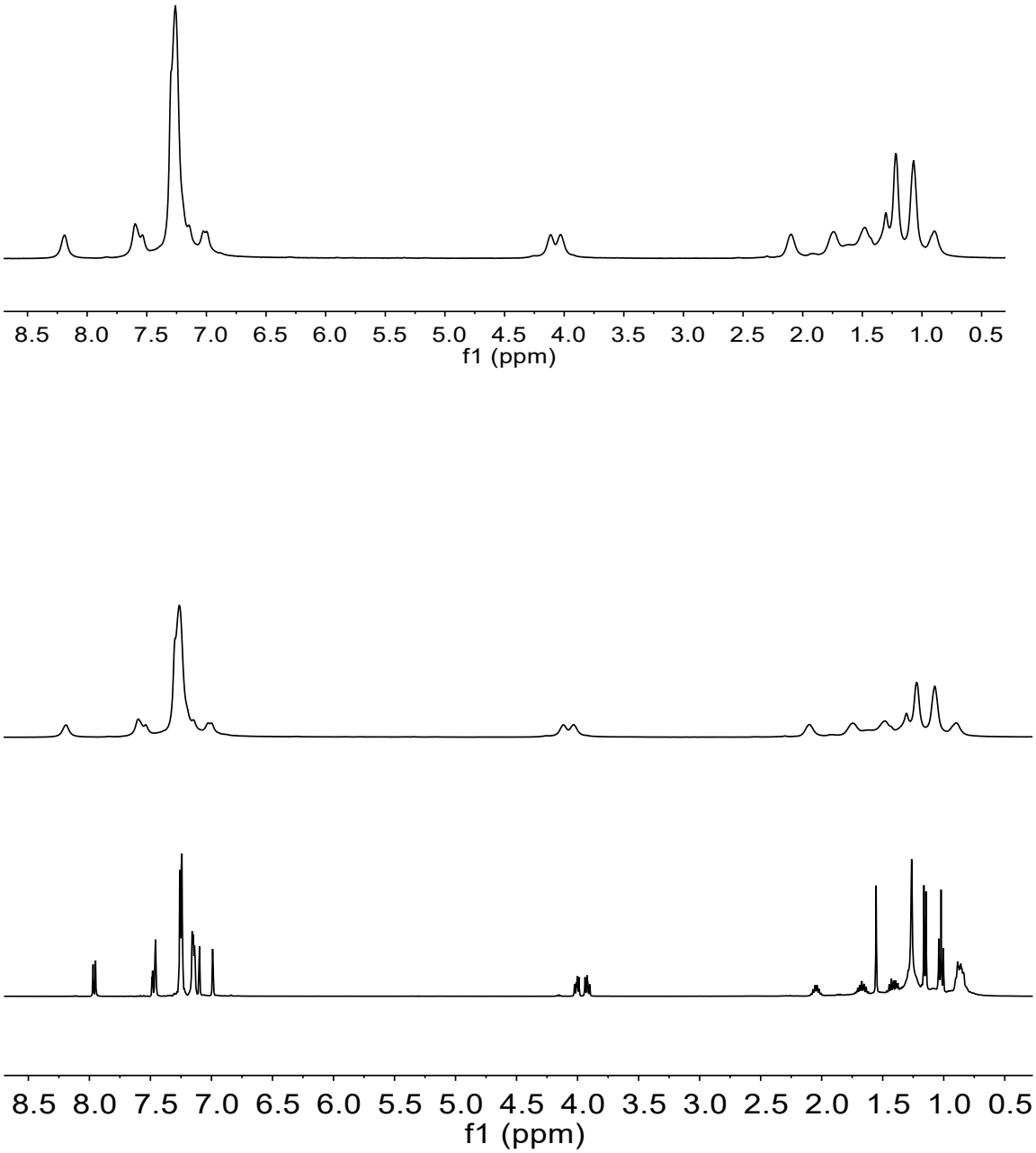

Figure S6. ^{1}H NMR spectrum of PChDPF and overlapping ^{1}H NMR spectra of monomer and corresponding polymer PChDPF in $CDCl_3$ (top: polymer, bottom:

monomer).

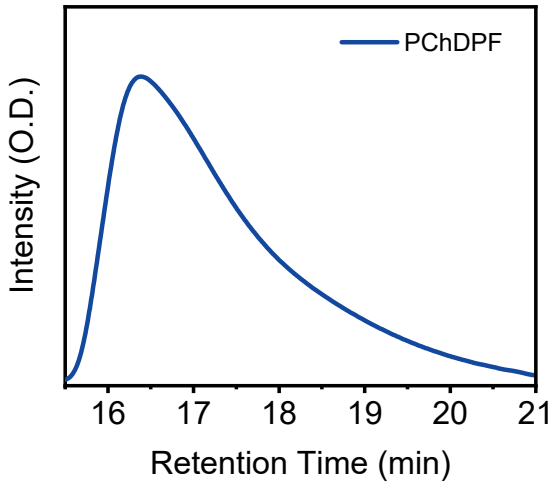

Figure S7. GPC curve of PChDPF.

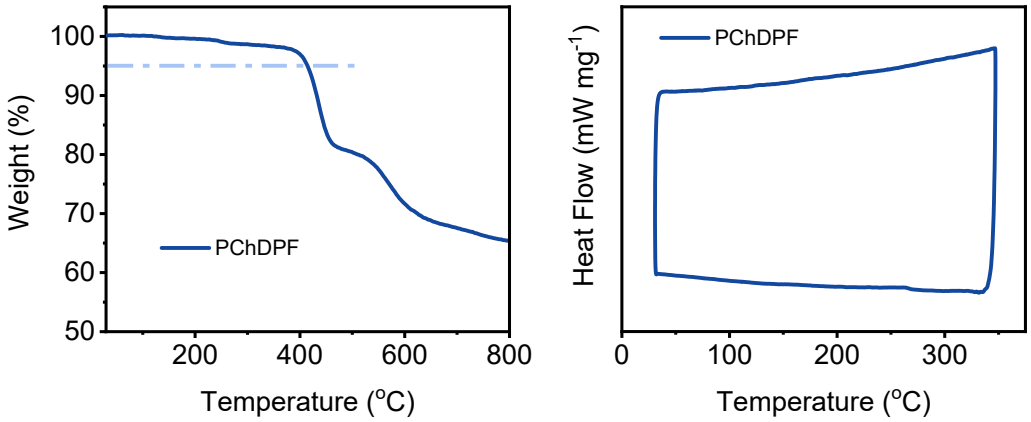

Figure S8. TG (left) and DSC (right) curves of PChDPF. Heating rate was 10 K min^{-1} under N_2 atmosphere.

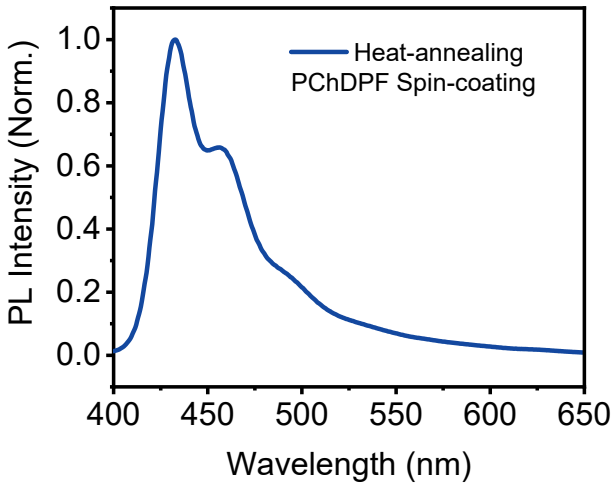

Figure S9. PL spectrum of PChDPF spin-coating film after heat-annealing.

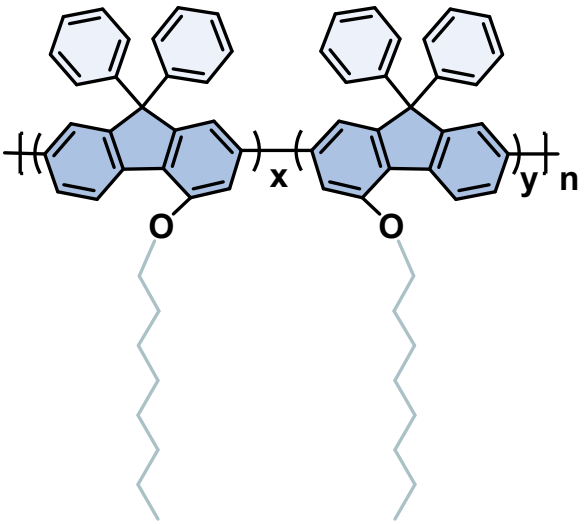

Scheme S2. Molecular formula of PODPF (contrast molecule).

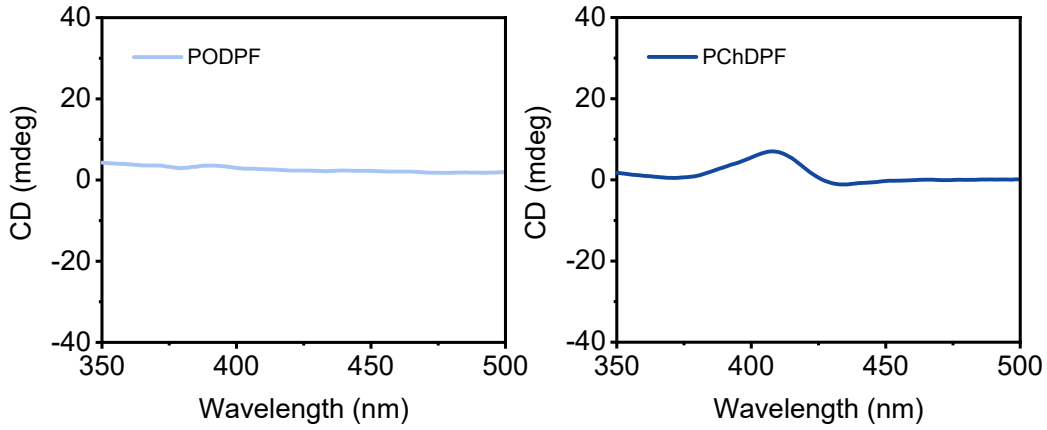

Figure S10. CD spectra of PChDPF and PODPF (contrast molecule) in toluene solution.

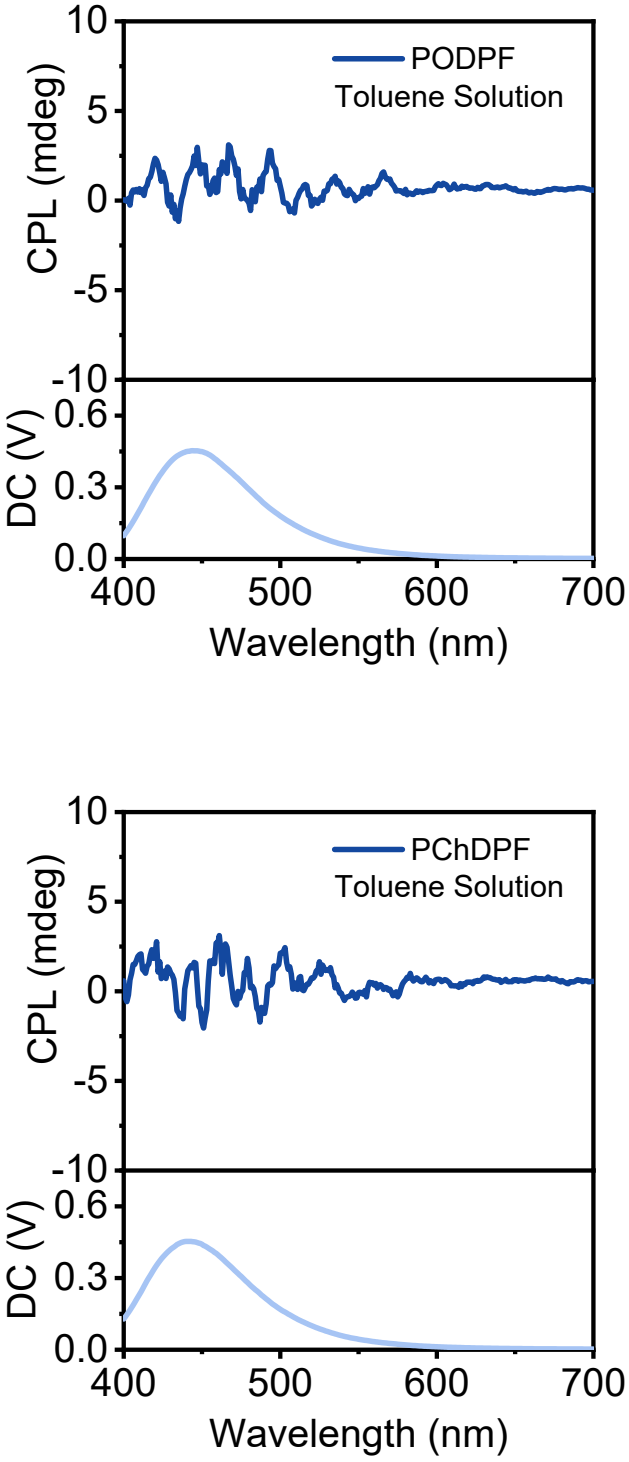

Figure S11. CPL spectra and DC curves of PChDPF and PODPF (contrast molecule) in toluene solution.

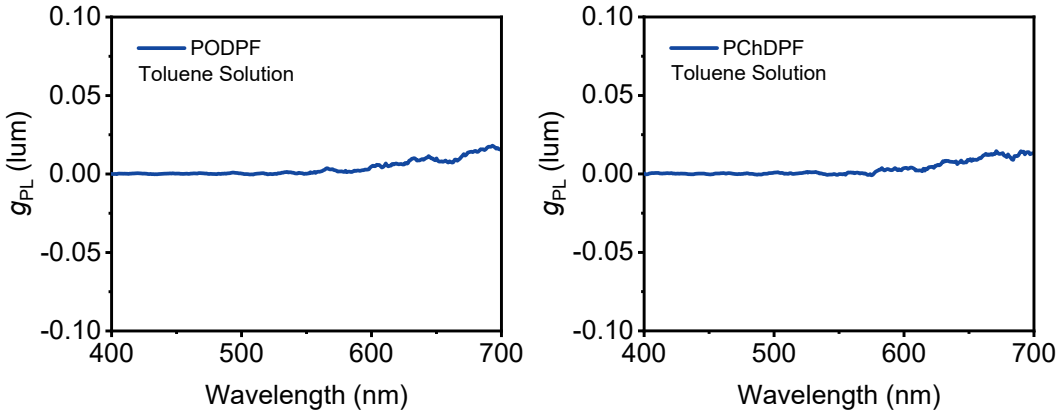

Figure S12. g_{lum} factors of PChDPF and PODPF (contrast molecule) in toluene solution.

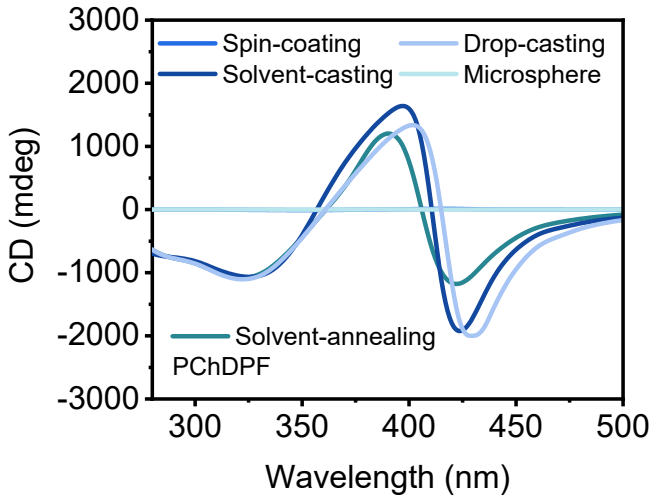

Figure S13. CD spectra of PChDPF in different self-assembly films.

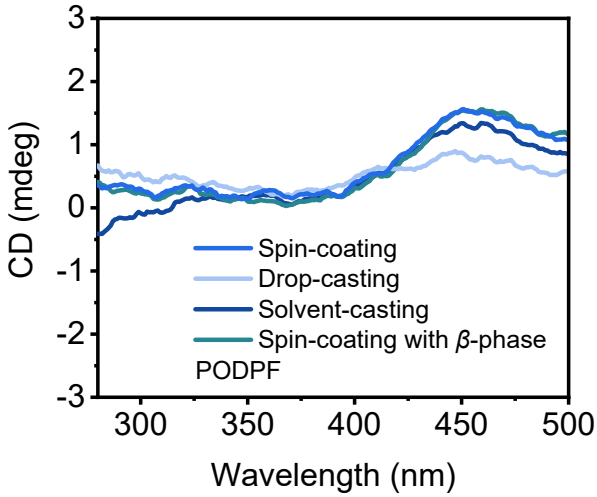

Figure S14. CD spectra of PODPF (contrast molecule) in different self-assembly films.

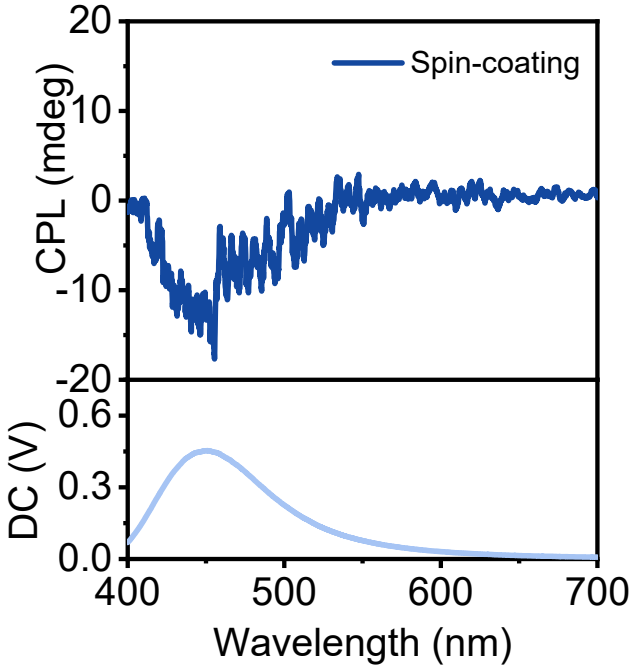

Figure S15. CPL spectrum and DC curve of PChDPF in spin-coating state.

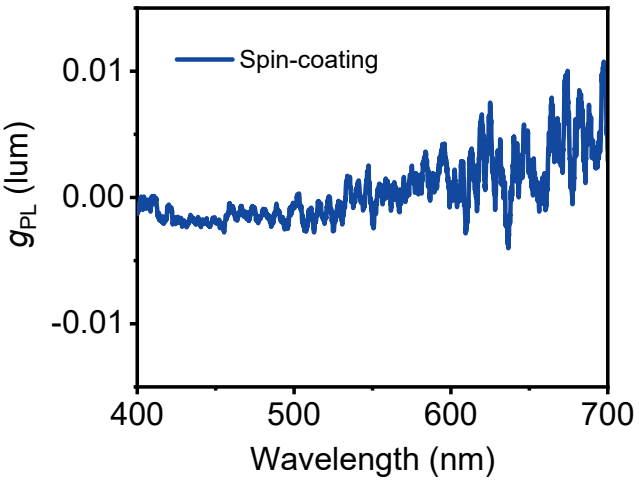

Figure S16. g_{lum} factors of PChDPF in spin-coating state.

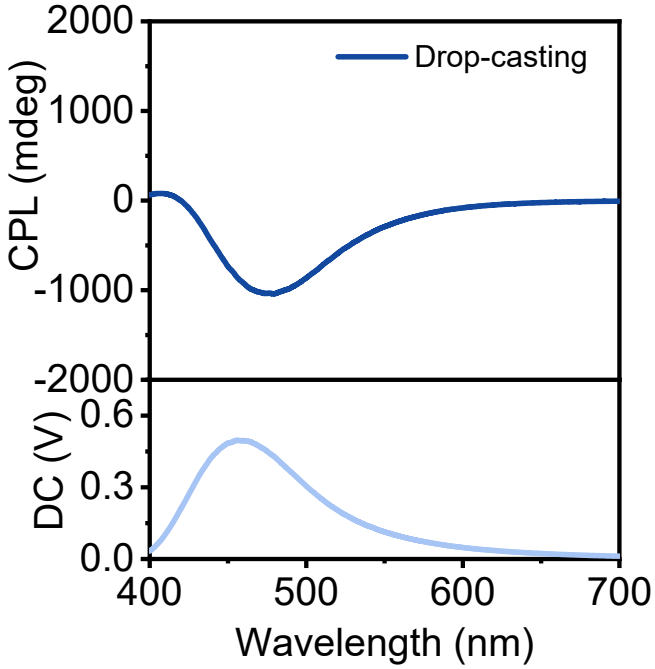

Figure S17. CPL spectrum and DC curve of PChDPF in drop-casting state.

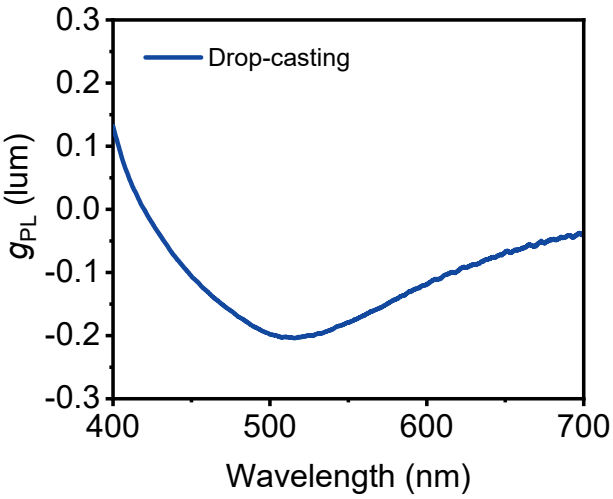

Figure S18. g_{lum} factors of PChDPF in drop-casting state.

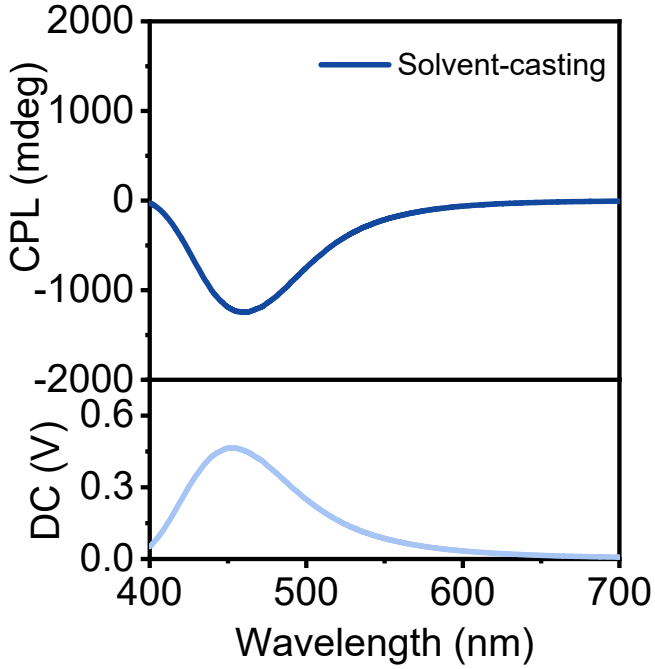

Figure S19. CPL spectrum and DC curve of PChDPF in solvent-casting state.

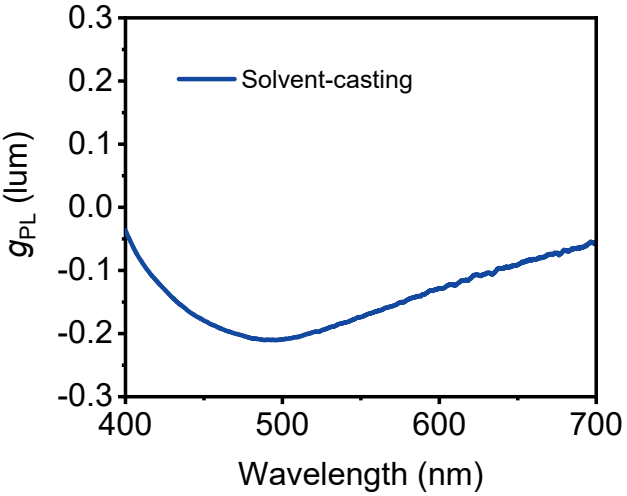

Figure S20. g_{lum} factors of PChDPF in solvent-casting state.

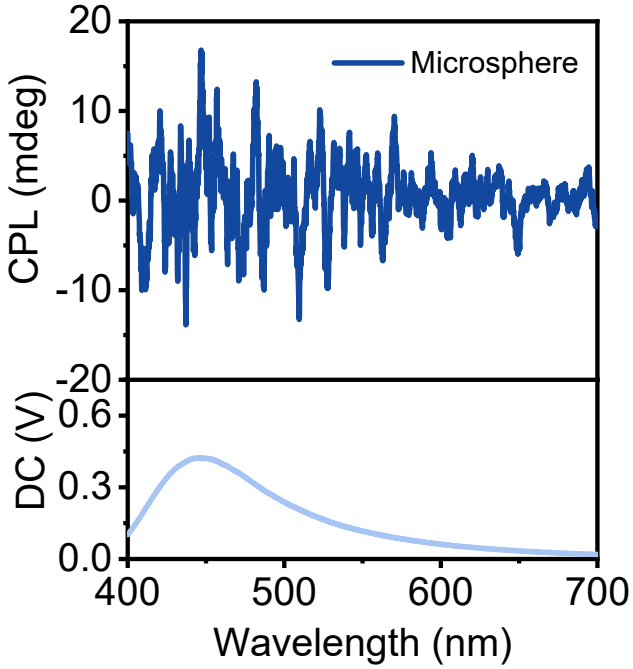

Figure S21. CPL spectrum and DC curve of PChDPF in microsphere film state.

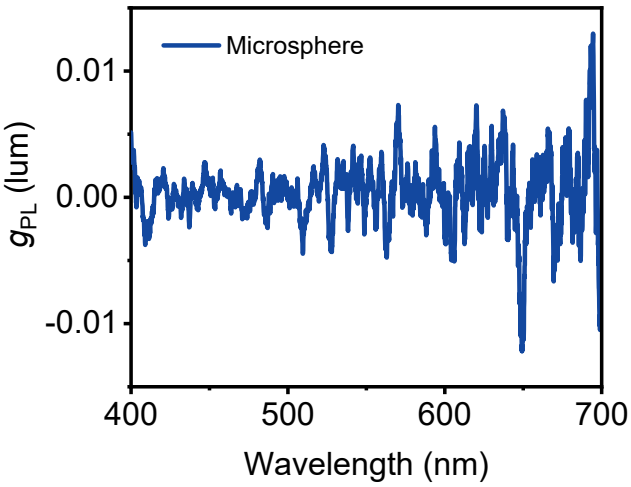

Figure S22. g_{lum} factors of PChDPF in microsphere film state.

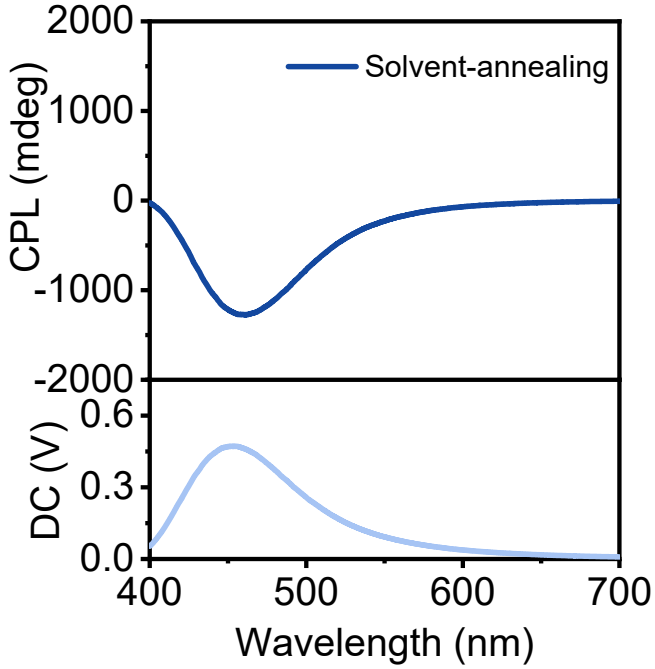

Figure S23. CPL spectrum and DC curve of PChDPF in solvent-annealing state.

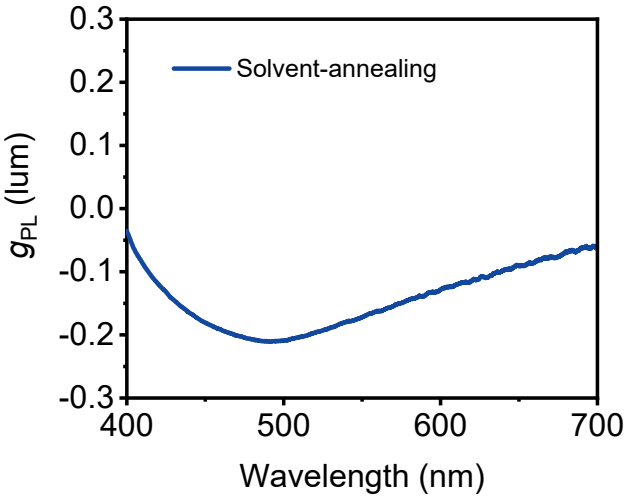

Figure S24. g_{lum} factors of PChDPF in solvent-annealing state.

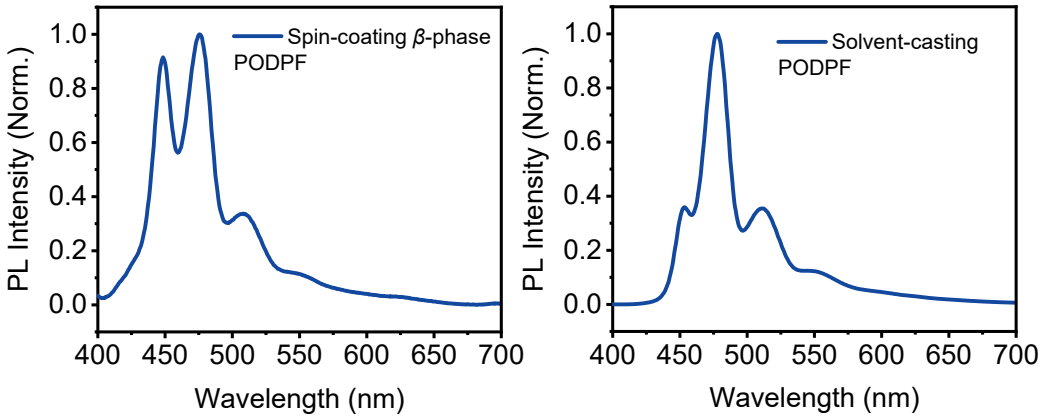

Figure S25. PL spectra of PODPF (contrast molecule) in spin-coating film with *β*-phase and solvent-casting states.

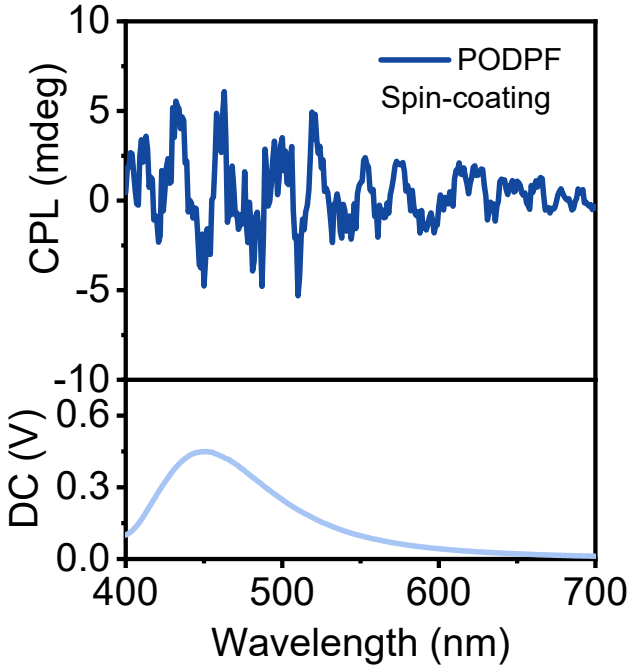

Figure S26. CPL spectrum and DC curve of PODPF (contrast molecule) in spin-coating state.

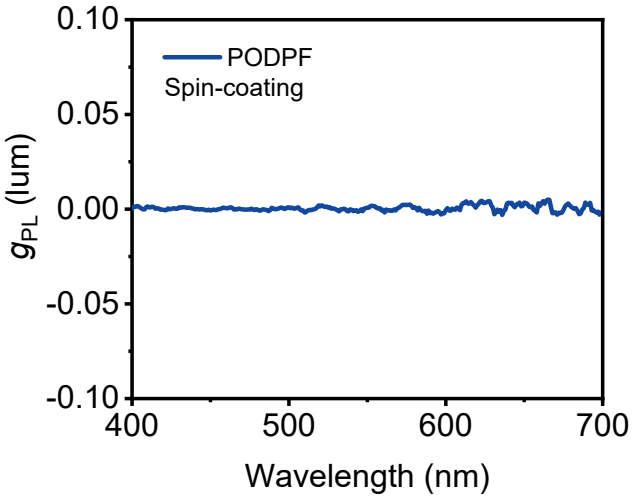

Figure S27. g_{lum} factors of PODPF (contrast molecule) in spin-coating state.

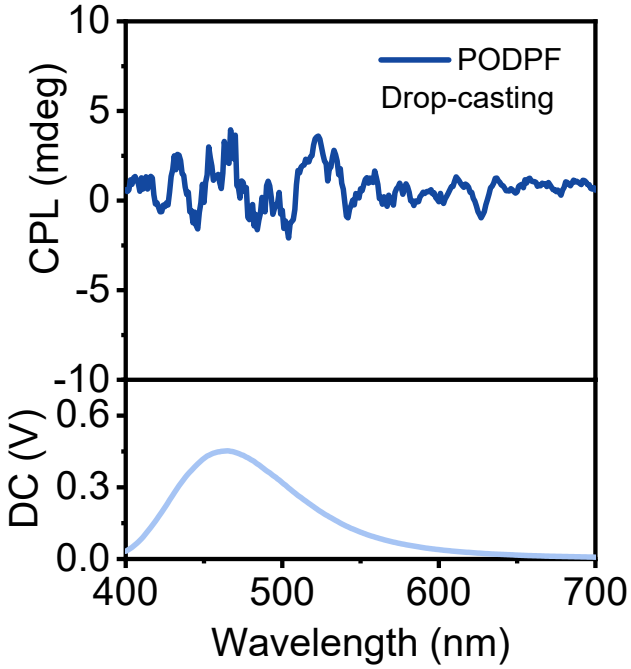

Figure S28. CPL spectrum and DC curve of PODPF (contrast molecule) in drop-casting state.

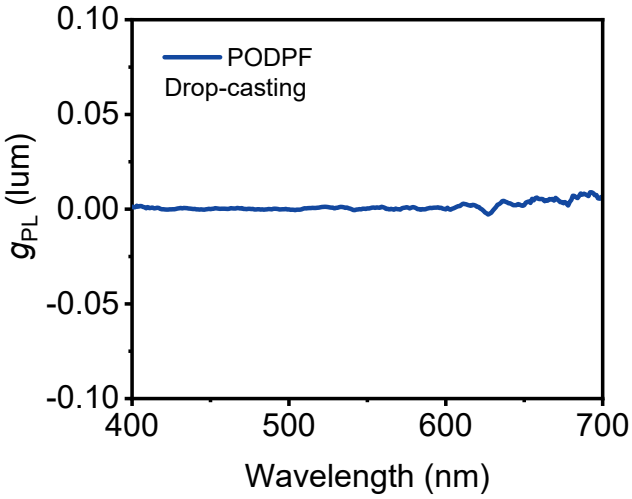

Figure S29. g_{lum} factors of PODPF (contrast molecule) in drop-casting state.

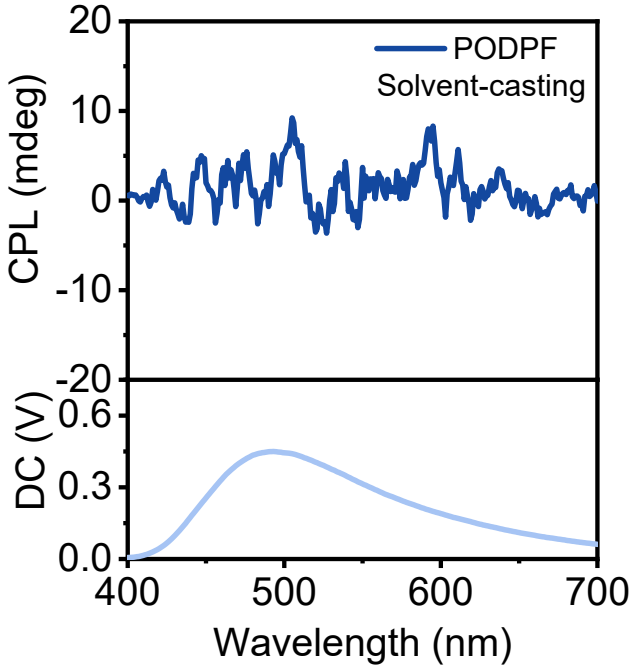

Figure S30. CPL spectrum and DC curve of PODPF (contrast molecule) in solvent-casting state.

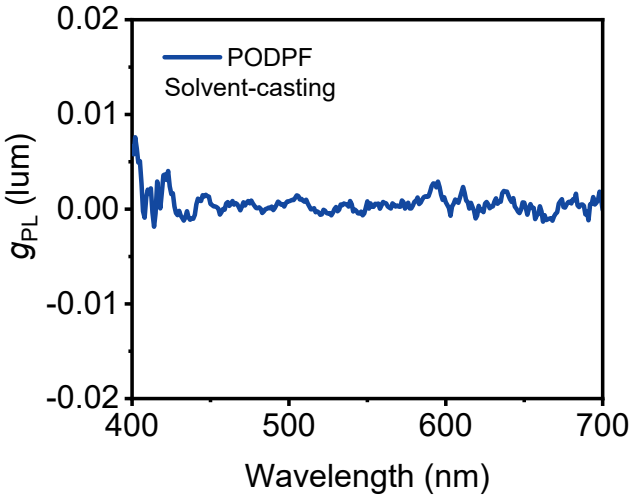

Figure S31. g_{lum} factors of PODPF (contrast molecule) in solvent-casting state.

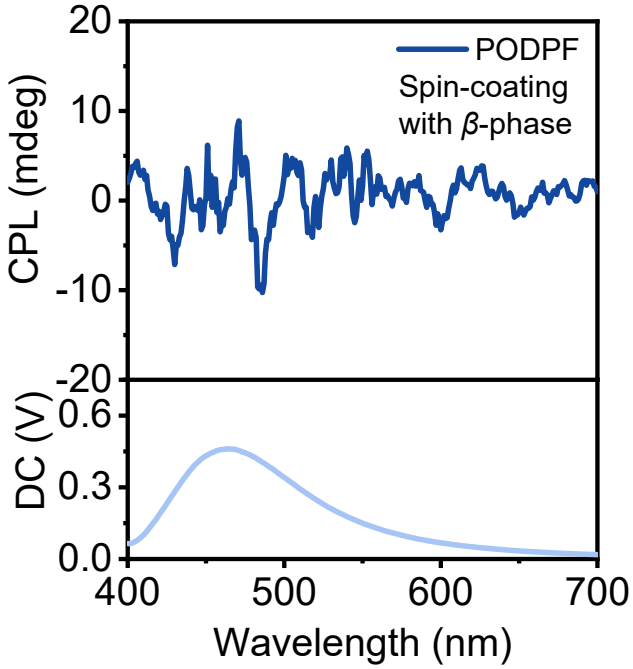

Figure S32. CPL spectrum and DC curve of PODPF (contrast molecule) in spin-coating film with *β*-phase.

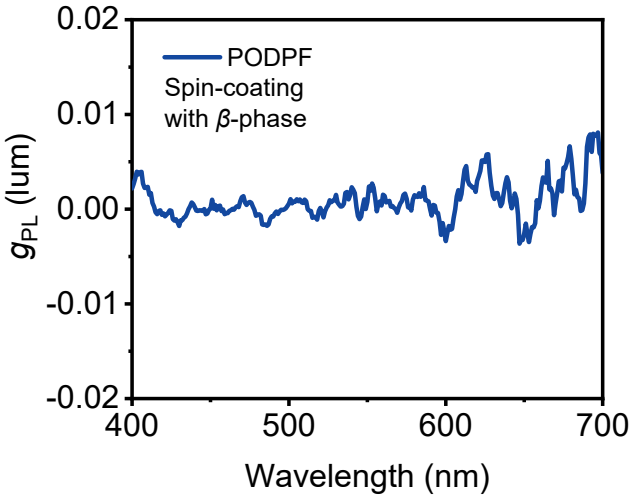

Figure S33. g_{lum} factors of PODPF (contrast molecule) in spin-coating film with *β*-phase.

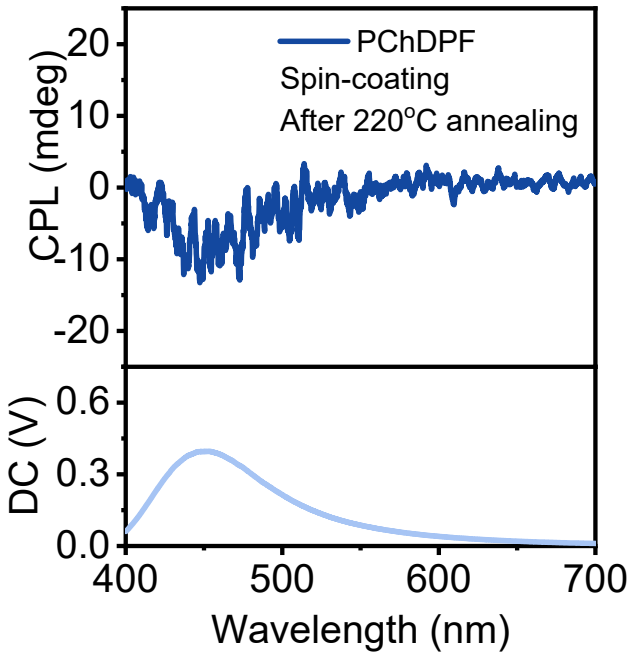

Figure S34. CPL spectrum and DC curve of PChDPF spin-coating film after heat annealing.

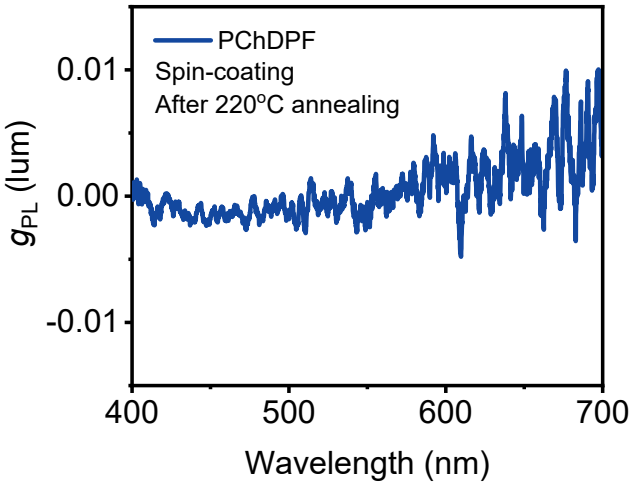

Figure S35. g_{lum} factors of PChDPF spin-coating film after heat annealing.

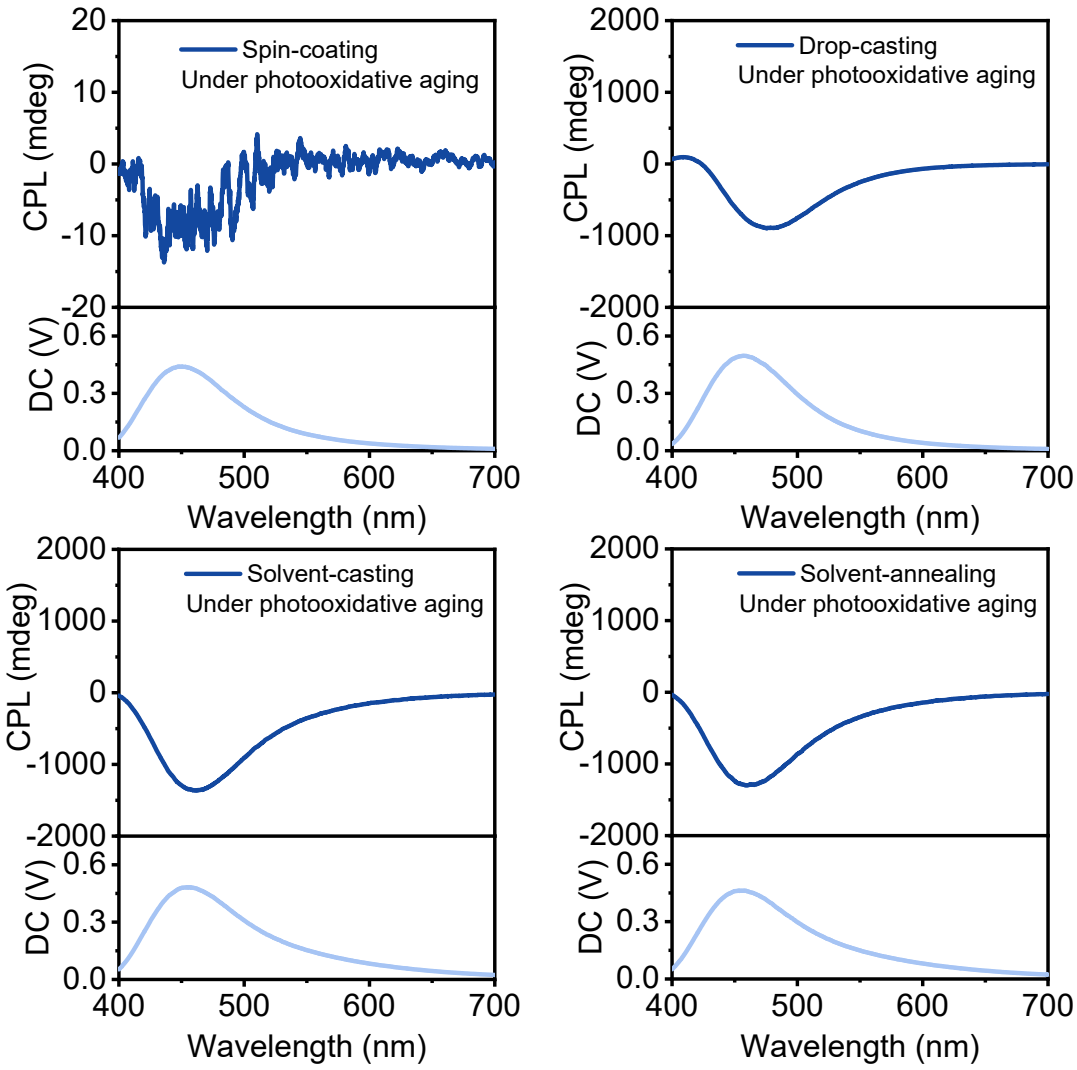

Figure S36. CPL spectra and DC curves of PChDPF in different assembly states under photooxidative aging for 24 hours.

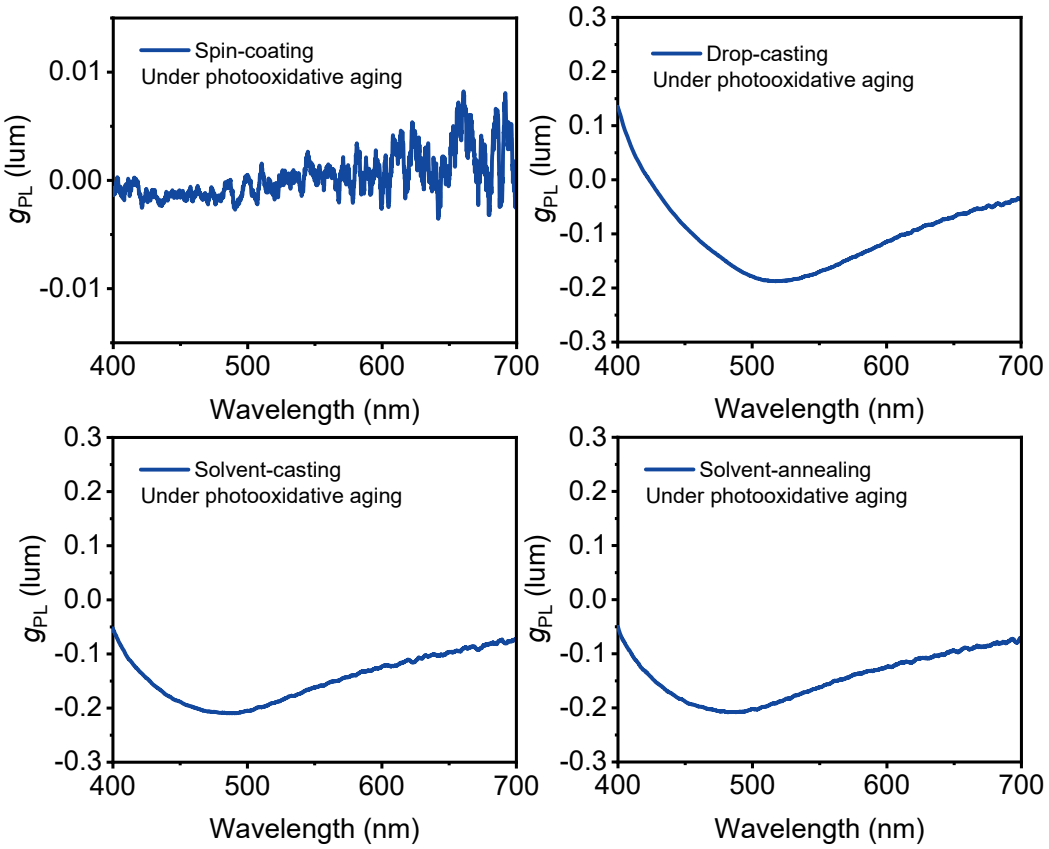

Figure S37. g_{lum} factors of PChDPF in different assembly states under photooxidative aging for 24 hours.

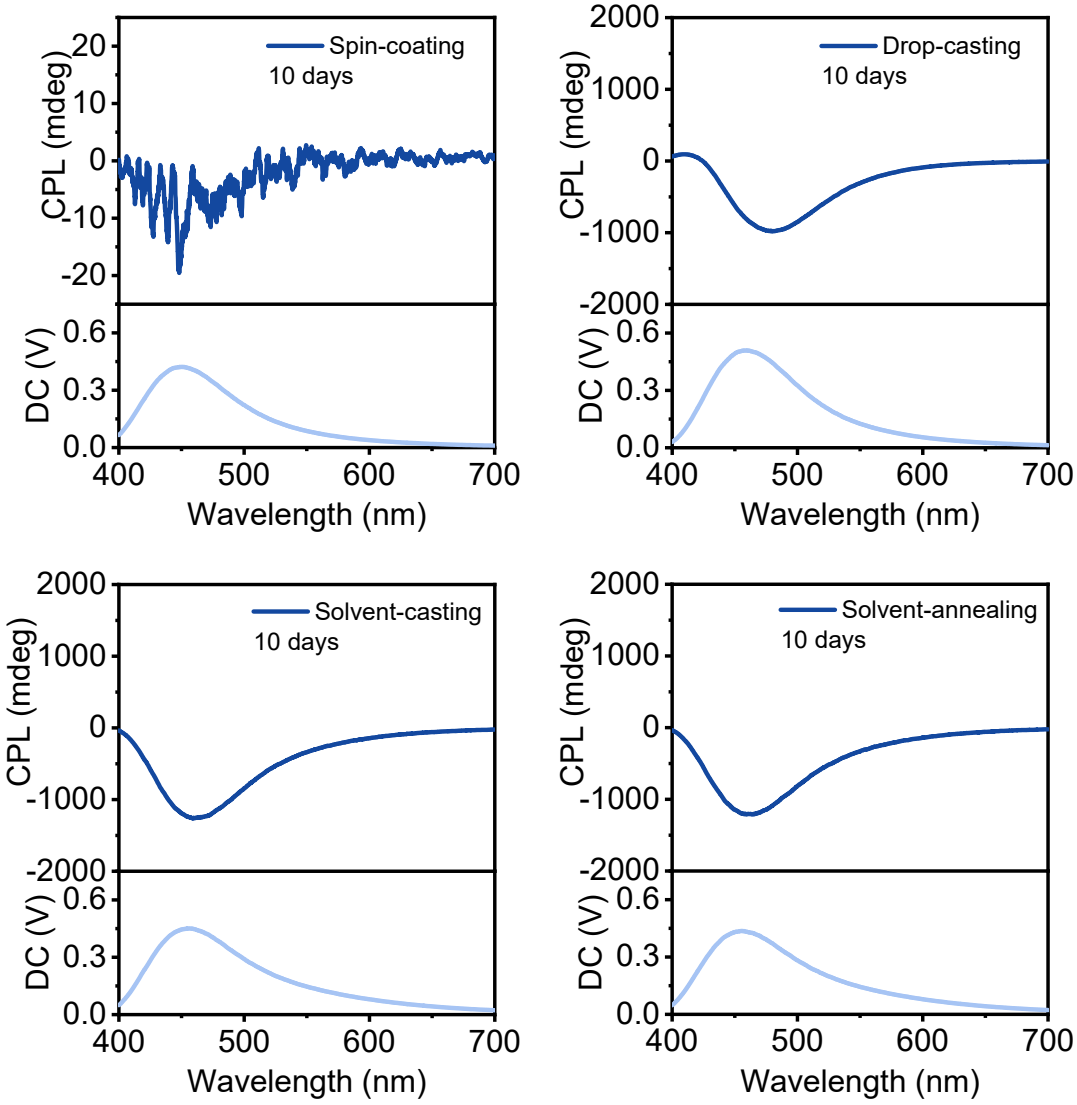

Figure S38. CPL spectra and DC curves of PChDPF in different assembly states at constant temperature and humidity for 10 days.

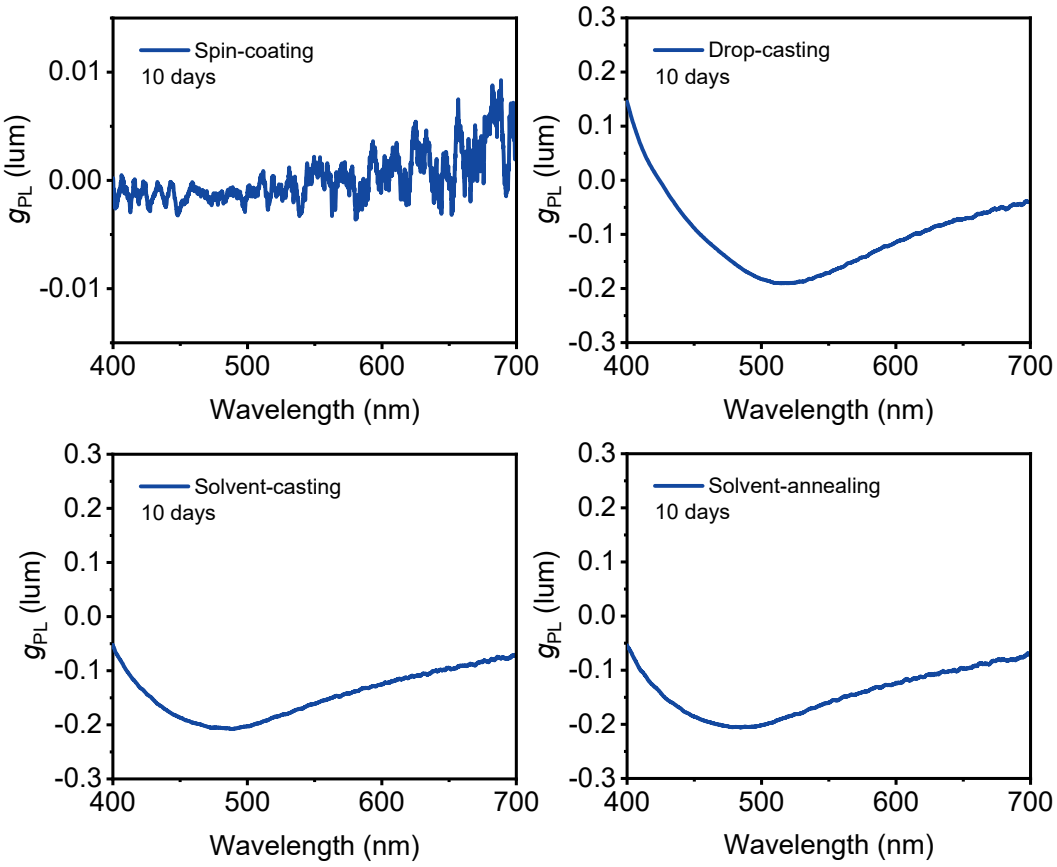

Figure S39. g_{lum} factors of PChDPF in different assembly states at constant temperature and humidity for 10 days.

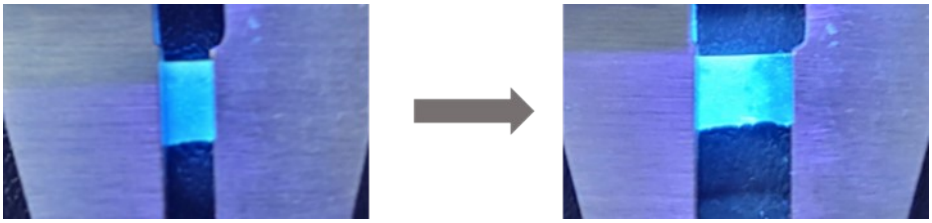

Figure S40. Pictures of PChDPF solvent-casting film combined with PDMS elastomers under tensile state.

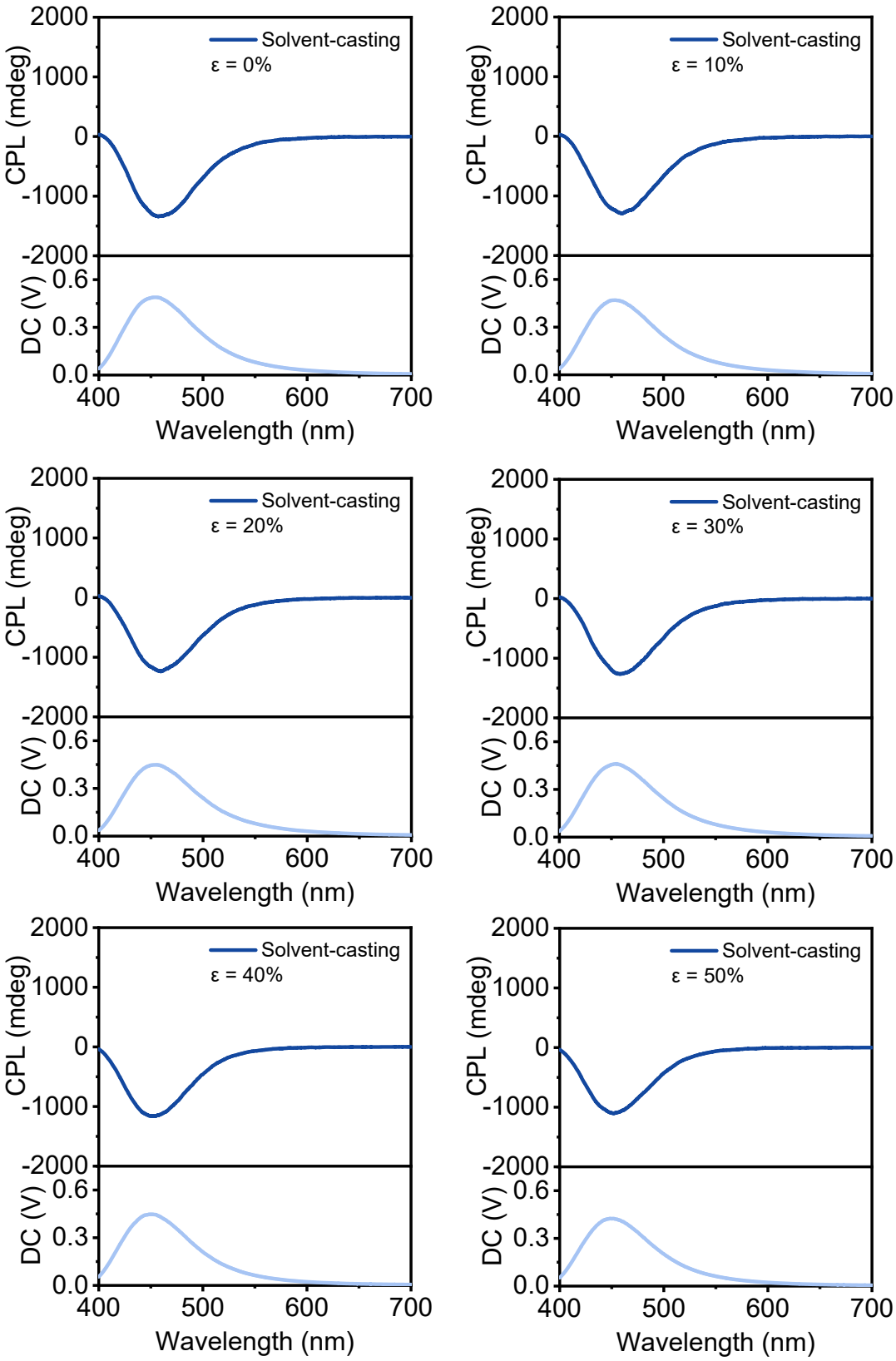

Figure S41. CPL spectra and DC curves of PChDPF solvent-casting film combined with PDMS elastomers under tensile state.

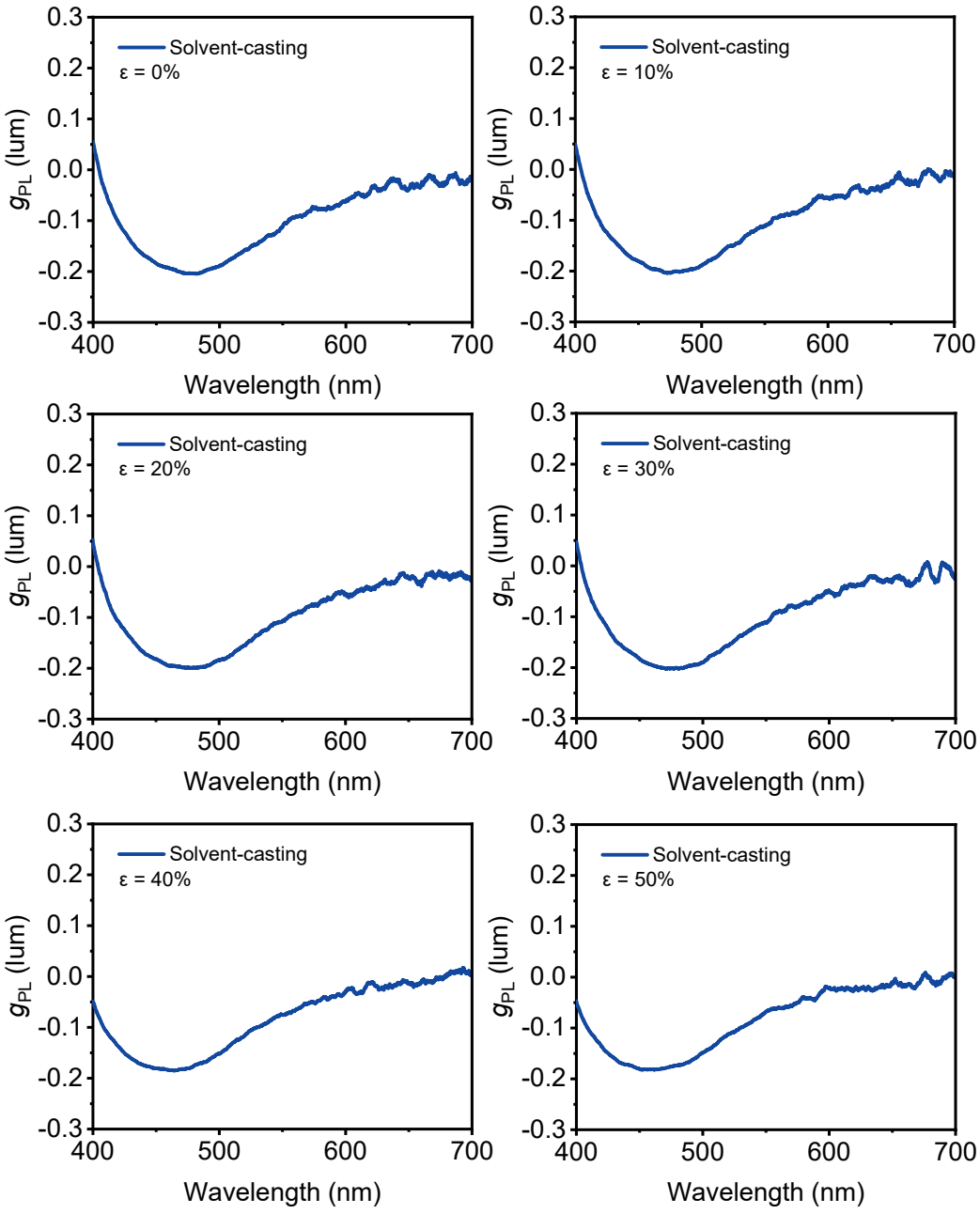

Figure S42. g_{lum} factors of PChDPF solvent-casting film combined with PDMS elastomers under tensile state.

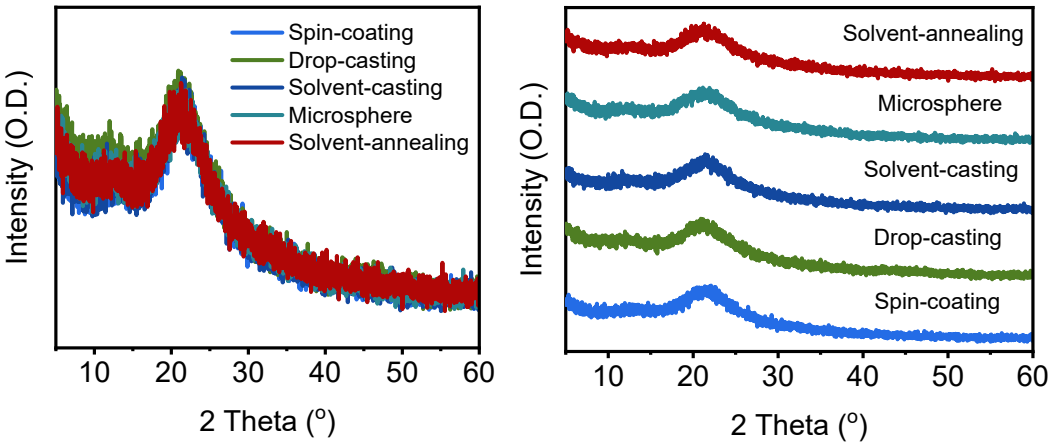

Figure S43. Powder X-ray diffraction spectra of PChDPF in different assembly states.

Figure S44. Light transmittance photographs of PChDPF in drop-casting (left) and solvent-casting (right) states.

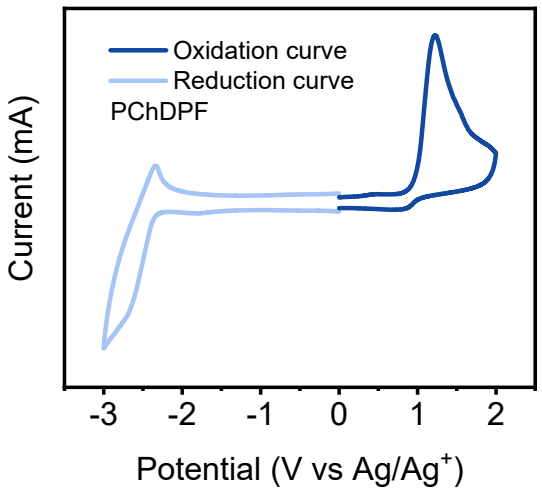

Figure S45. Cyclic voltammograms curves of PChDPF under N_2 atmosphere.

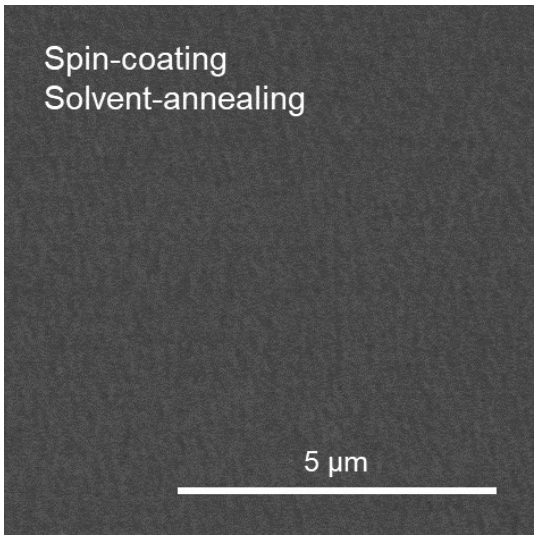

Figure S46. SEM image of PChDPF in solvent-annealing after spin-coating state.

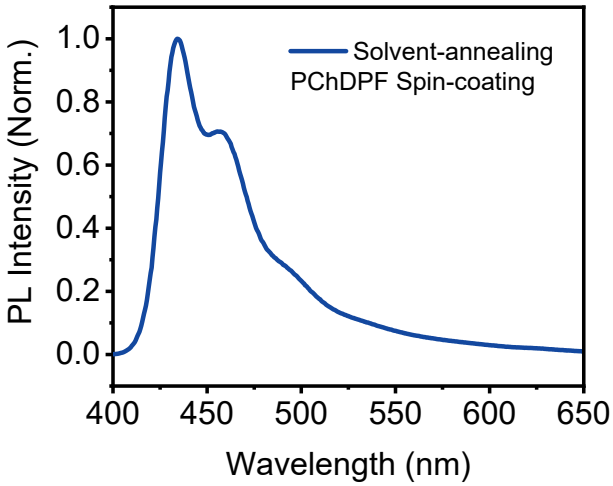

Figure S47. PL spectrum of PChDPF in solvent-annealing after spin-coating state.

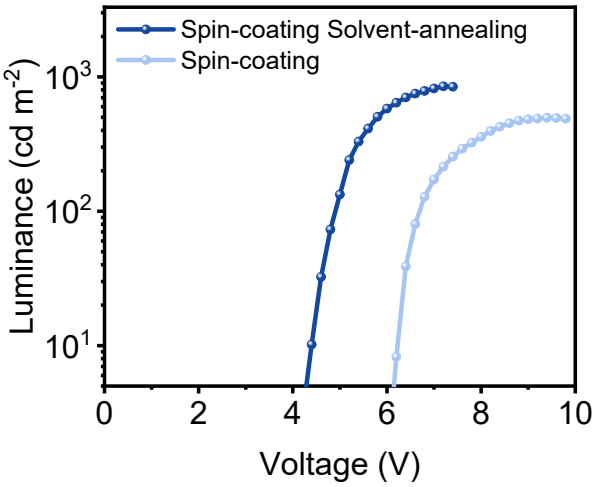

Figure S48. Luminance-voltage characteristics of PChDPF-based PLEDs manufactured by spin-coating and solvent-annealing after spin-coating.

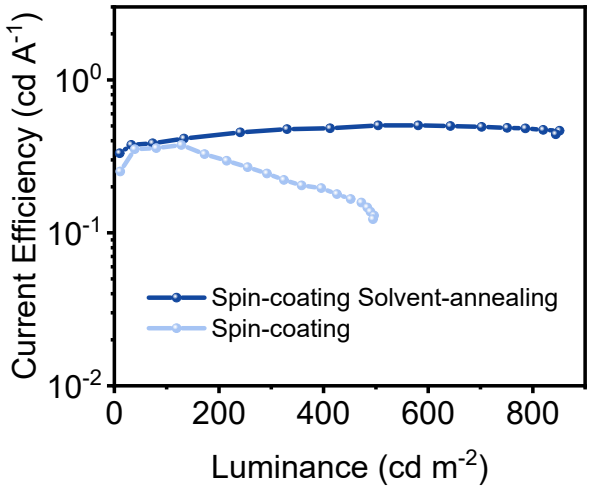

Figure S49. Luminance versus current efficiency spectra of PChDPF-based PLEDs manufactured by spin-coating and solvent-annealing after spin-coating.

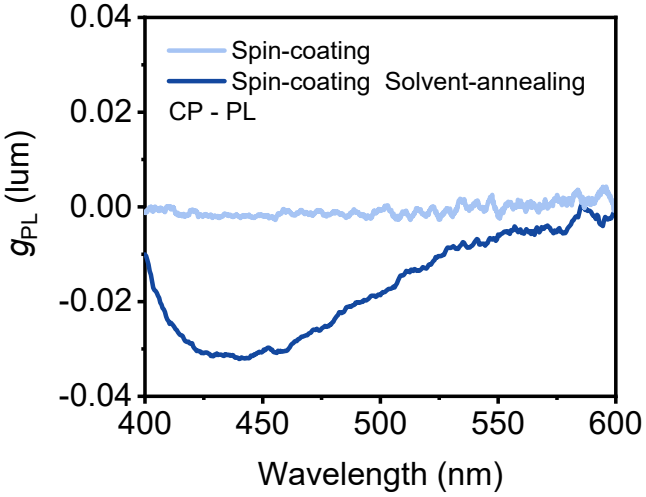

Figure S50. g_{lum} factors of PChDPF in spin-coating film and solvent-annealing after spin-coating film (CP-PL).

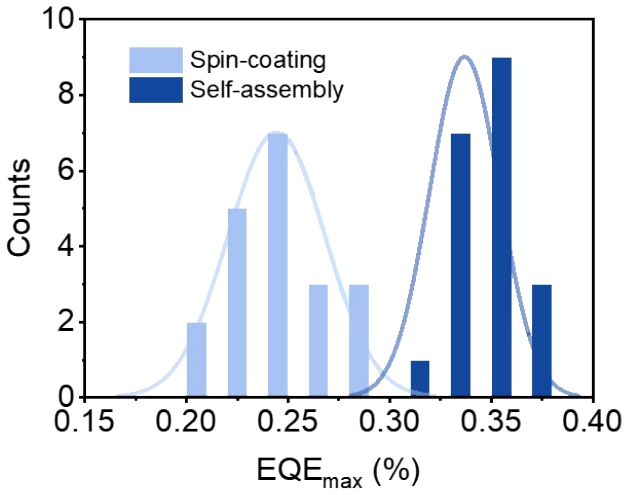

Figure S51. External quantum efficiency statistics of PChDPF spin-coating and self-assembled PLED devices.

References

1 J. Lin, W. Zhu, F. Liu, L. Xie, L. Zhang, R. Xia, G. Xing, W. Huang, *Macromolecules* 2014, **47**, 1001−1007.

2 N. Sun, Y. Han, L. Sun, M. Xu, K. Wang, J. Lin, C. Sun, J. An, S. Wang, Q. Wei, Y. Zheng, Z. Zhuo, L. Bai, L. Xie, C. Yin, X. Zhang, W. Huang, *Macromolecules* 2021, **54**, 6525−6533.